Atmospheric Environment 43 (2009) 3460–3466

Contents lists available at ScienceDirect

Atmospheric Environment

journal homepage: www.elsevier.com/locate/atmosenv

Properties and sources of individual particles and some chemical species in the aerosol of a metropolitan underground railway station

Imre Salma [a,*], Mihály Pósfai [b], Kristóf Kovács [c], Ernő Kuzmann [a], Zoltán Homonnay [a], József Posta [d]

[a] Institute of Chemistry, Eötvös University, P.O. Box 32, H-1518 Budapest, Hungary
[b] Department of Earth and Environmental Sciences, University of Pannonia, Veszprém, Hungary
[c] Institute of Materials Science, University of Pannonia, Veszprém, Hungary
[d] Department of Inorganic and Analytical Chemistry, Debrecen University, Debrecen, Hungary

ARTICLE INFO

Article history:
Received 1 February 2009
Received in revised form
19 April 2009
Accepted 21 April 2009

Keywords:
Underground railways
Iron
Chromium
Hematite
Speciation
Individual particles
Surface properties
Health effects

ABSTRACT

Aerosol samples in $PM_{10-2.0}$ and $PM_{2.0}$ size fractions were collected on the platform of a metropolitan underground railway station in central Budapest. Individual aerosol particles were studied using atomic force microscopy, scanning electron microscopy and transmission electron microscopy with energy-dispersive X-ray spectrometry and electron diffraction. The bulk aerosol samples were investigated by ^{57}Fe Mössbauer spectroscopy, and they were subjected to chemical speciation analysis for Cr. The particles were classified into groups of iron oxides and iron, carbonates, silicates, quartz and carbonaceous debris. Electron micrographs showed that the Fe-rich particles in the $PM_{2.0}$ size fraction typically consisted of aggregates of nano-sized hematite crystals that were randomly oriented, had round shapes and diameters of 5–15 nm. In addition to hematite, a minor fraction of the iron oxide particles also contained magnetite. In addition, the $PM_{2.0}$-fraction particles typically had a rugged surface with layered or granular morphologies. Mössbauer spectroscopy suggested that hematite was a major Fe-bearing species in the $PM_{10-2.0}$ size fraction; its mass contribution to the Fe was 36%. Further constituents (ferrite, carbides and FeOOH) were also identified. The water soluble amounts of Cr for the underground railway station and city center were similar. In the $PM_{10-2.0}$ size fraction, practically all dissolved Cr had an oxidation state of three, which corresponds to ambient conditions. In the $PM_{2.0}$ size fraction, however, approximately 7% of the dissolved Cr was present as Cr(VI), which was different from that for the urban aerosol. It is suggested that the increased adverse health effects of aerosol particles in metros with respect to ambient outdoor particles is linked to the differences in the oxidation states, surface properties or morphologies.

1. Introduction and objectives

Underground railway systems transport millions of passengers per day in a number of cities around the world. They represent a unique microenvironment within cities due to their closed character and restricted ventilation, lack of photochemistry, specific emission sources and meteorological conditions. Several studies have considered aerosols or air quality in the underground railways in various cities. A review and an account on the physical and chemical properties and behaviour of the aerosol particles, as well as their major emission sources and health implications were given by Nieuwenhuijsen et al. (2007 and references therein) and Salma (2009 and references therein), respectively. The studies consistently showed elevated pollution levels in terms of particulate mass that was usually several times higher than for the outdoor areas above the stations. Furthermore, the average chemical composition and size distributions of the particles in the underground railways differed from those of the outdoor urban aerosol. The particles were larger and heavier, and were mainly composed of Fe (Sitzmann et al., 1999). The largest enrichment factors were usually observed for Fe, Mn, Ni, Cu and Cr, while black carbon was depleted. Mechanical wear and friction of electric conducting rails and collectors, brake pads, ordinary rails and wheels, as well as erosion of construction material and resuspension were identified as the major emission sources (Salma, 2009).

The transition metals listed above can be of concern because travelling in metros can considerably increase commuters' daily exposures to them for persons who are not subject to occupational exposure (Pfeifer et al., 1999; Chillrud et al., 2004). Some transition metals have documented negative health effects at high concentrations including carcinogenicity, gene mutations and neurotoxicity (ATSDR, 2000; WHO, 2000; HEI, 2002). The health impacts

* Corresponding author.
E-mail address: salma@chem.elte.hu (I. Salma).

1352-2310/$ – see front matter © 2009 Elsevier Ltd. All rights reserved.
doi:10.1016/j.atmosenv.2009.04.042

due to excess exposure to these transition metals are thought to be caused – in large part – by free ions and redox-active sites on the surface, available to take part in Fenton chemistry to generate free hydroxyl radicals in the body, resulting in oxidative stress and inflammation (Gilmour et al., 1996; Donaldson et al., 1997; Seaton et al., 2005; Ayres et al., 2008). It was concluded from standard in vitro toxicological tests using cultured alveolar human lung epithelial cell line A549 that the cytotoxicity of aerosol particles collected in a metro system was comparable to welding fume particles, larger than for TiO_2 particles, and appreciably smaller than for high doses of quartz particles (Seaton et al., 2005). The genotoxicity of metro particles was also studied by assessing their ability to cause mitochondrial depolarization and to form intracellular reactive oxygen species (ROS) in cultured epithelial cell line A549 (Karlsson et al., 2005, 2008). The effects of several types of real PM_{10} aerosol samples were compared, including particles collected on a busy street, in a tire road wear simulator, from wood and diesel smoke, and metal oxide and metal powders (Fe_3O_4 and CuO with particle diameters <5 μm, and Zn–70%Cu alloy with a particle diameter <50 μm). It was concluded that the underground aerosol particles were approximately eight times more genotoxic and four times more likely to cause oxidative stress than the particles collected on a busy street (Karlsson et al., 2005). Nevertheless, it also turned out that the metro particles damaged the mitochondria similarly to the other aerosol types investigated, and, therefore, their higher genotoxicity is not explained by special damage mechanisms. The intracellular ROS may be part of the explanation since a statistically significant difference was observed for the aerosol sample collected in the underground railway with respect to the other samples. At the same time, the powder samples and the water or citrate extracts (modelling intracellular mobilization) of the Fe_3O_4 powder did not cause by far as much DNA damage as the underground samples, and did not increase the oxidative DNA damage (Karlsson et al., 2008). Therefore, it can be expected that the chemical forms of the transition metals in the aerosol particles and their capability to release radicals play a role in their increased adverse health effects. Further information on the chemical species and oxidation states of the transition metals (mainly of Fe) for underground railway systems is highly desirable. It has to be also noted that the health effects of particulate transition metals at low and intermediate concentrations are unknown, as well as the cumulative impacts of their concurrent exposures.

In a previous study, temporal variations of the PM_{10} mass concentration and meteorological parameters were determined with high time resolution, and the aerosol mass, elemental composition and aerosol properties in separate $PM_{10-2.0}$ and $PM_{2.0}$ size fractions were derived for the Budapest metro (Salma et al., 2007). As a continuation of the research, we report and interpret in this work the results obtained from the aerosol samples by speciation analyses for Fe and Cr, and by a variety of microscope methods for individual particles. We discuss the implications for the source processes and health effects of the particles in underground railway systems in general.

2. Methods

The aerosol sampling was performed on the platform of the Astoria station in the Budapest metro. The sampling device was set up at the far end of the platform ca. 2 m in front of the control cabinet and ca. 1.5 m from the wall of the platform. The sampling inlet was placed at a height of 2.5 m. This location was chosen as a compromise between meeting conditions for undisturbed measurement and obstructing pedestrian traffic as little as possible. It was assumed that the concentration gradient close to the sampler was small, since the air is presumably mixed by trains moving along the platform and by ventilation.

The samples were collected using a stacked-filter unit sampler. The device contains two 47-mm-diameter Nuclepore polycarbonate membrane filters with pore sizes of 8 μm (Apiezon-coated, coarse filter) and 0.4 μm (fine filter) in series in an NILU-type open-face stacked-filter cassette (Maenhaut et al., 1994). Upstream of the filter cassette, there is a pre-impaction stage with its inlet facing down. The sampler is designed to operate at an airflow rate of 16–17 l min^{-1}, at which the aerosol particles are separated into $PM_{10-2.0}$ and $PM_{2.0}$ size fractions. Two aerosol sample pairs were collected, one from 12:30 local daylight saving time (UTC + 2 h) on 20 April 2006 (Thursday) to 05:45 the next day, and the other from 06:00 to 15:00 on 21 April 2007 (Friday). A pair of field filter blanks was also taken. The sampling artifacts that could modify the abundance of some chemical species during the collections are expected to be small because of the lack of photochemistry and low levels of ozone. The samples were placed in polycarbonate Petri dishes and were stored in a refrigerator until analysis. Additional details on the sampling location, instrumentation, samples, experimental procedures and conditions can be found in Salma et al. (2007).

Quarter sections of the filters were studied by individual particle analysis, i.e., by scanning electron microscopy (SEM), transmission electron microscopy (TEM), and atomic force microscopy (AFM). For the SEM and AFM studies, the membrane filters were used directly, without any sample preparation. The particles investigated with TEM were transferred from the membrane filter onto a Formvar-coated Cu support grid by placing the grid onto the filter and applying a few drops of ethanol to wash the particles over onto the grid surface. Scanning electron microscopy was performed using a Philips XL30 ESEM instrument (The Netherlands) with an acceleration voltage of 20 kV in backscatter and secondary electron modes. Transmission electron microscopy images and selected-area diffraction (SAED) patterns were obtained using a Philips CM20 instrument (The Netherlands) with an acceleration voltage of 200 kV. The compositions of selected particles were determined using energy-dispersive X-ray spectrometry in both SEM and TEM. Atomic force microscopy measurements were performed using a Molecular Imaging PicoScan instrument (USA) in magnetic AC mode. From the AFM scans, topography, amplitude and phase data were displayed and recorded simultaneously. The fine filters were studied by all three microscope methods, whereas the coarse filters were investigated by SEM only.

The coarse filters were investigated by ^{57}Fe Mössbauer spectroscopy (Kuzmann et al., 2003). The specimens were prepared from the filters cut in sections with an area of approximately 2 cm^2, and five layers of the filter sections were put on top of each other to increase the effective thickness. We used γ-rays with an energy of 14.4 keV that were provided by a ^{57}Co/Rh radioactive source with an activity of 3×10^9 Bq. The measurements were performed in transmission geometry with a conventional Mössbauer spectrometer (WissEl, Germany) working in a constant acceleration mode at temperatures of 20 K in a close circuit refrigerator He cryostat and at 297 K. The Mössbauer spectra were recorded for one week each and were fitted using the MossWinn computer code (Klencsár et al., 1996).

Half sections of one of the coarse and one of the fine filters were subjected to speciation analysis in order to determine the abundances of Cr(III) and Cr(VI). The applied analytical procedure was described earlier (Posta et al., 1993). In short, a quarter filter section was extracted in 20 cm^3 high purity Milli-Q water at a temperature of 363 K for 1 h in order to dissolve Cr(VI). For the determination of total soluble Cr(III) and Cr(VI), another quarter section of the same filter was treated by microwave-assisted digestion (Milestone MLS1200 Mega Microwave Laboratory System) in a closed Teflon vessel with 4 cm^3 concentrated nitric

acid (p.a.) and 1 cm^3 concentrated hydrogen peroxide (p.a.). The extracts were filtered through a 0.22-μm syringe PVDF membrane filter (Millipore, USA) to remove the filter debris and suspended insoluble particles. The solutions were analyzed using a graphite furnace atomic absorption spectrometer (Perkin Elmer Analyst 600, USA) at a wavelength of 357.9 nm, using Zeeman background correction. Calibration solutions were prepared from Scharlau stock solution. For both cases, blank filter samples were also treated and analyzed, and the blank values were subtracted from the corresponding data for the real filters.

3. Results and discussion

3.1. Shape and types of the aerosol particle, emission sources for the $PM_{10-2.0}$ size fraction

Images of particles in the $PM_{10-2.0}$ size fraction obtained by SEM and TEM typically showed irregular and angular shapes, suggesting that they originated from primary emission sources (Fig. 1a and b). Many particles of the $PM_{2.0}$ size fraction had similar shapes as the coarse particles. Atomic force microscopy images showed that the $PM_{2.0}$-fraction particles typically had a rather rugged surface and appeared to have either layered or granular morphologies (Fig. 2). The surfaces of the most common particles typically exhibited globular features with diameters in the 10–50 nm range, larger than the crystal grains observed by TEM and Mössbauer spectroscopy (see Sections 3.2 and 3.3, respectively). Energy-dispersive X-ray spectrometry revealed that the dominant elements were Fe and O in most particles in both the $PM_{10-2.0}$ and $PM_{2.0}$ size fractions. Some further elements were observed in other particles. The particles were classified in five groups that are each characterized by large concentrations of: 1) Fe and O, 2) Ca, Mg and C, 3) Si, Ca, Mg, Cl and Fe, 4) Si, and 5) C. The compositions of the groups are consistent with particles of iron oxides, carbonates, silicates, quartz and carbonaceous (possibly plastic and anthropogenic) debris, respectively. The particles of group 2 occasionally contained sulphate as well. Special attention was devoted to detecting alloying metals of steel (Mn, Ni or Cr) in Fe-rich particles but none of these could be identified.

The main source of particles in the $PM_{10-2.0}$ size fraction belonging to group 1 was the mechanical wear of moving parts made of iron or steel (electric conducting and regular rails, electric collectors, brake pads, wheels), while the $PM_{10-2.0}$-fraction particles associated with groups 2–4 could originate from wind erosion and weathering of construction material (concrete) and minerals. It is thought that resuspension of the dust particles caused by the turbulent mixing of the air due to the moving trains plays a significant role in the aerosol generation.

3.2. Crystal structure, Fe species and sources of Fe-rich particles in the $PM_{2.0}$ size fraction

Transmission electron microscopy images with larger magnification and SAED patterns were obtained for the thinner parts or transparent edges of the Fe-rich $PM_{2.0}$-fraction particles. A Fe-rich particle is displayed in Fig. 3. The images reveal that all these particles are aggregates of nano-sized crystal grains. The grains had round shapes with fairly uniform diameters between approximately 5–15 nm. The variation in contrast between individual crystals is caused by diffraction effects. Grains with darker contrast had a crystallographic zone axis nearly parallel to the electron beam. Selected-area diffraction patterns exhibited diffraction rings, indicating the polycrystalline nature of the aggregates and a random crystallographic orientation of the nanocrystals. The structures of the nanocrystals were identified on the basis of lattice spacings measured from the diffraction rings. All diffraction patterns obtained from iron oxide particles contained rings that were consistent with the structure of hematite (Fe_2O_3, space group R3c, $a = 5.04$ Å, $c = 13.8$ Å) (Fig. 4a). In addition, the most intense reflections of magnetite (Fe_3O_4, space group Fd3m, $a = 8.40$ Å) were also present in a few patterns (Fig. 4b). Thus, hematite was the major phase in all iron oxide particles, and in some particles, minor amounts of magnetite were also present. In few cases, the iron oxide phases occurred internally mixed within aerosol particles. The presence of other possible Fe oxides could not be excluded because some of their diffraction maxima could overlap with those of hematite; nevertheless, they could only be present in an insignificant amount with respect to hematite. Hematite is the major component of rust. However, it is unlikely that the hematite nanocrystals were formed by corrosion processes because iron(III) oxyhydroxides (such as goethite and lepidocrocite) – phases that should have been also formed in the reaction with water vapour – were not identified in the $PM_{2.0}$ size fraction, and because corrosion is expected to generate coarse aerosol particles. Instead, it is thought that these aggregated Fe-rich aerosol particles were emitted by sparking between the electric conducting (third) rail and collectors.

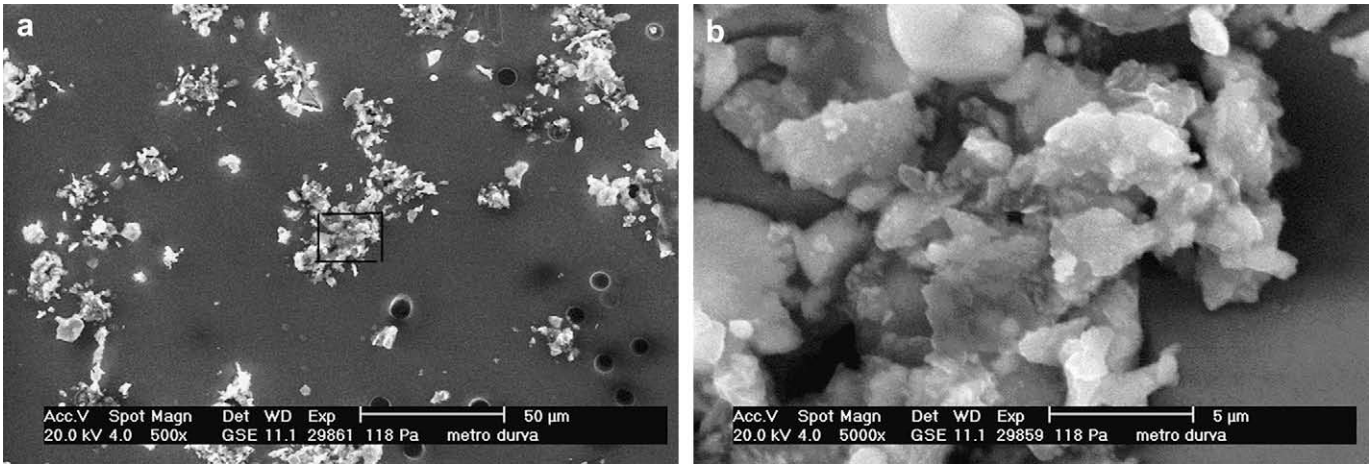

Fig. 1. Secondary electron images of aerosol particles in a sample collected in a metropolitan underground railway station. The boxed area in Panel a is shown enlarged in Panel b.

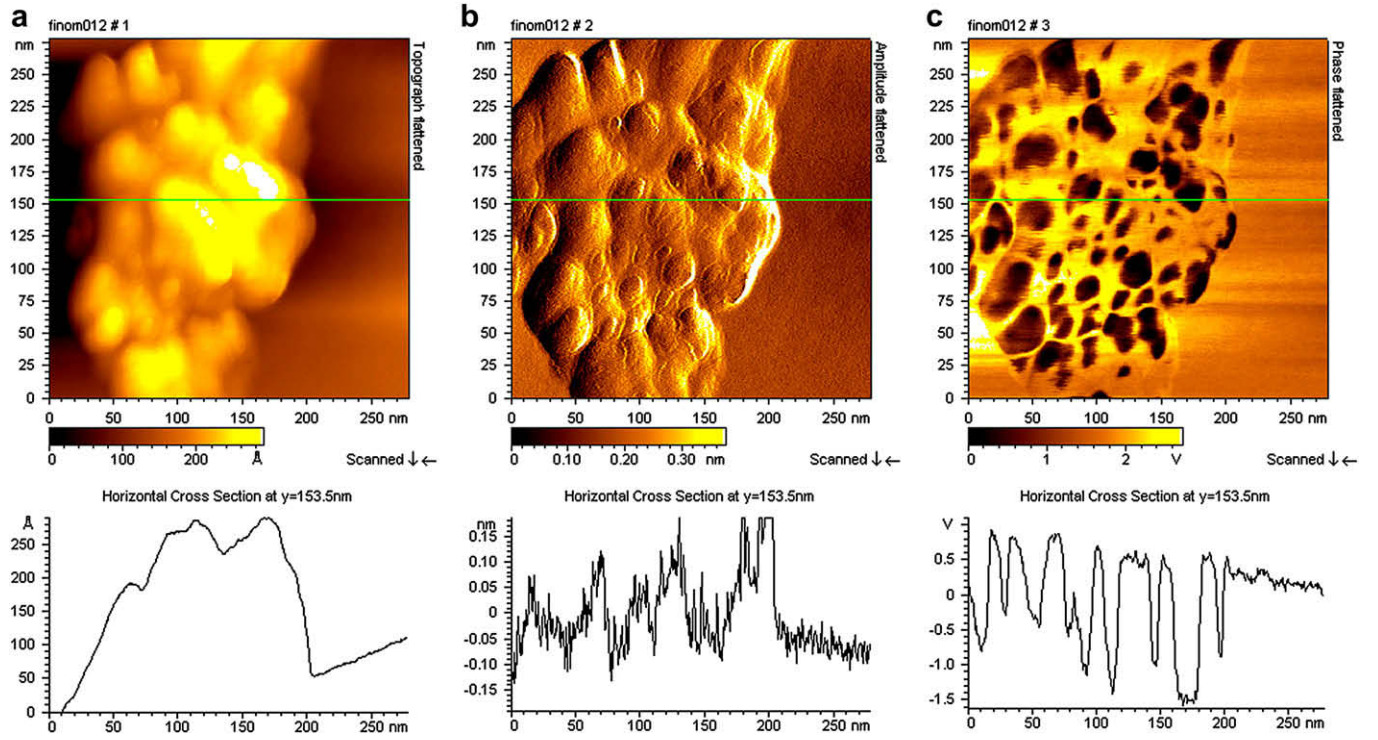

Fig. 2. Atomic force microscopy images obtained with an oscillating cantilever from an aerosol particle, presumably an iron oxide, in the $PM_{2.0}$ size fraction. Topographic (a), amplitude (b) and phase images (c), each with a corresponding profile along the green horizontal line. The profile under the topographic image (a) indicates that the particle is ca. 25 nm thick, and the bumps on its surface are about 5–10 nm high.

3.3. *Iron species in the $PM_{10-2.0}$ size fraction*

Mean atmospheric concentration of Fe in the $PM_{10-2.0}$ size fraction was 34 μg m^{-3} (in the $PM_{2.0}$ size fraction, it was 15.5 μg m^{-3}, Salma et al., 2007). Its amount that originated from the Earth's crust ($m(Fe)_{crust}$) can be estimated as:

$$m(\mathrm{Fe})_{\mathrm{crust}} = \left(\frac{m(\mathrm{Fe})}{m(\mathrm{Si})}\right)_{\mathrm{crust}} m(\mathrm{Si})_{\mathrm{aerosol}}, \quad (1)$$

where $m(Si)_{aerosol}$ is the concentration of Si in the aerosol particles, and $m(X)_{crust}$ represents the concentration of element X in Mason's average crustal rock (Mason and Moore, 1982). The calculation was performed with two geogenic elements, i.e., with Si and then with Ti. It is implicitly assumed in the evaluation that Si or Ti in the $PM_{10-2.0}$ size fraction mainly originate from crustal emission sources in the metro which is a reasonable assumption since their mean crustal enrichment factors (EFs) calculated relative to Mason's average crustal rock composition with Al as the reference element was 1.2 and 1.6, respectively (Salma et al., 2007). It was calculated in this way that at most 2% of the Fe mass can be associated with the crustal emission sources. This implies that the dominating amount of Fe originated from specific emission sources, and, therefore, the relative abundance of its chemical species is of interest.

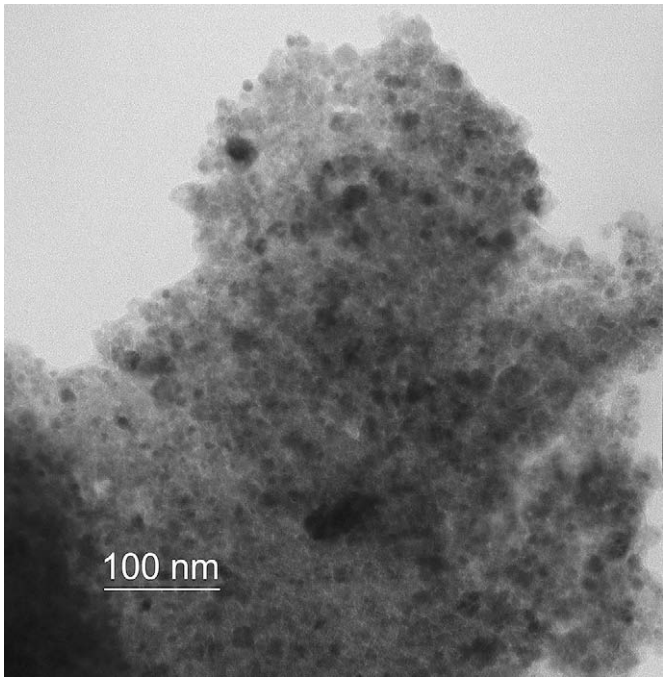

Fig. 3. Bright-field transmission electron microscope image of a hematite (Fe_2O_3) particle from a metropolitan underground railway station, showing nano-sized crystal grains.

The ^{57}Fe Mössbauer spectrum for the $PM_{10-2.0}$ filter taken at a temperature of 20 K is shown in Fig. 5. The spectral envelope exhibits a central paramagnetic part and a large magnetically split contribution. It was decomposed into five sextets (denoted as S1–S5) and two doublets (denoted as D1 and D2). The Mössbauer parameters of the components are shown in Table 1. The isomer shifts were determined relative to α-Fe. The sextet S1 is a major component of the spectrum with a relative amount of 36%. Based on its isomer shift, quadrupole splitting and hyperfine field (Stevens and Stevens, 1969–1990), it was associated with α-Fe_2O_3 (hematite). The Mössbauer parameters of the sextets S2 and S3 can be linked to the Fe(III) and Fe(II) components of Fe_3O_4 (magnetite) below the Vervey temperature of 110 K, when Fe(III) and Fe(II)

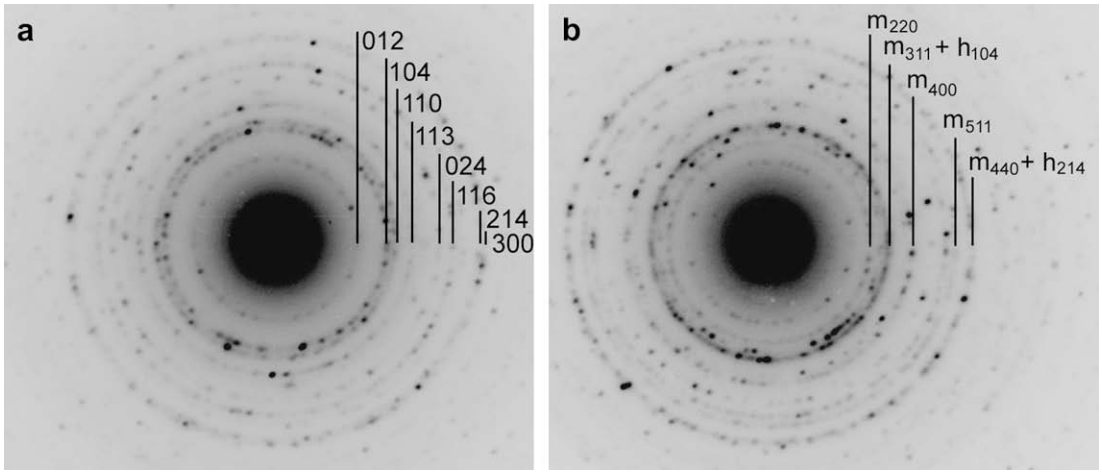

Fig. 4. Selected-area electron diffraction patterns of a hematite (a) and a mixed hematite/magnetite particle (b). The diffraction rings indicate that both particles contain randomly oriented nanocrystals. The Miller indices of hematite corresponding to each ring are indicated in (a), whereas only the additional magnetite reflections (marked by m) are indicated in (b). The unmarked diffraction rings belong to hematite.

microenvironments at the octahedral cation site of the lattice are separated in the spectrum. The isomer shift and hyperfine field of the sextet S4 reflect undoubtedly α-Fe (ferrite). The sextet S5 is a minor component and can be attributed to Fe_3C (cementite), considering its typical hyperfine field. The doublets D1 and D2 can be assigned to paramagnetic and/or superparamagnetic FeOOH and paramagnetic Fe–Mn carbides since the Mössbauer parameters derived were close to their reported values. For example, the carbide $(Fe_{1-x}Mn_x)_3C$ with $x > 0.3$ is paramagnetic at and above 20 K. The Mössbauer spectrum obtained at room temperature (RT) also confirmed the assignments. The presence of the subspectrum of α-Fe at RT was more obvious than for 20 K. The Mössbauer parameters of the main sextet at RT can also correspond to hematite. The changes in the paramagnetic part of the spectra for both 20 and 295 K clearly indicate the presence of some superparamagnetic phase. This can be associated with FeOOH, most likely in the form of goethite, but γ-FeOOH (lepidocrocite) can also occur. The grain size of superparamagnetic phases occurring at 20 K can be estimated to be smaller than or close to 8 nm. A small amount of well-crystallized, non-superparamagnetic goethite can also be identified in the spectrum at RT, though its magnetically split subspectrum for 20 K can strongly overlap with that of hematite. For the same reason, the presence of another FeOOH phase, such as akaganeite or lepidocrocite, cannot be entirely excluded. Previous Mössbauer studies indicated the presence of oxyhydroxides as dominant iron-bearing phases in ambient aerosol samples (e.g., Kopczewicz and Kopczewicz, 2002). It has to be noted that quantitative phase analysis from the spectrum derived at room temperature represents difficulties because the relative spectral areas of the components cannot give accurately the relative abundance of the phases, since the

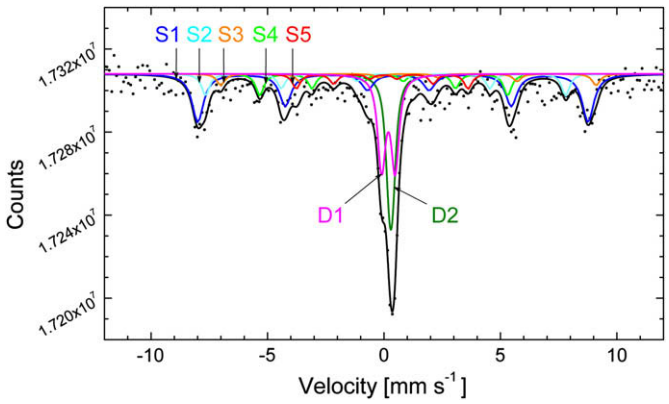

Fig. 5. Mössbauer spectrum recorded at a temperature of 20 K for $PM_{10-2.0}$ size fraction aerosol particles collected in a metropolitan underground railway station. The components are S1: α-Fe_2O_3 (hematite), S2 and S3: Fe_3O_4 (magnetite), S4: α-Fe (ferrite), S5: Fe_3C (cementite), D1 and D2: paramagnetic and superparamagnetic FeOOH and Fe–Mn carbides. The arrows denote the first line of the components.

Table 1
Mössbauer parameters at 20 K of the $PM_{10-2.0}$-fraction aerosol sample collected in a metropolitan underground railway station.

Component property [unit]	Value	Assignment
Sextet S1		α-Fe_2O_3 (hematite)
Area [%]	36	
Isomer shift [mm s^{-1}]	0.54	
Magnetic field [T]	51.69	
quadrupole splitting [mm s^{-1}]	−0.23	
Sextet S2		Fe_3O_4 (magnetite)
Area [%]	7.6	
Isomer shift [mm s^{-1}]	0.21	
Magnetic field [T]	50.79	
Sextet S3		
Area [%]	4.0	
Isomer shift [mm s^{-1}]	1.05	
Magnetic field [T]	49.98	
Sextet S4		α-Fe (ferrite)
Area [%]	9.1	
Isomer shift [mm s^{-1}]	−0.07	
Magnetic field [T]	33.00	
Sextet S5		Fe_3C (cementite)
Area [%]	6.3	
Isomer shift [mm s^{-1}]	0.06	
Magnetic field [T]	22.83	
Quadrupole splitting [mm s^{-1}]	−0.05	
Doublet D1		Paramagnetic and
Area [%]	20	superparamagnetic
Isomer shift [mm s^{-1}]	0.21	FeOOH and paramagnetic
Quadrupole splitting [mm s^{-1}]	0.58	Fe–Mn carbides
Doublet D2		
Area [%]	17	
Isomer shift [mm s^{-1}]	0.31	
Quadrupole splitting [mm s^{-1}]	0.14	

corresponding relative Mössbauer–Lamb factors are unknown (Vértes et al., 1979). However, the ratio of the Mössbauer–Lamb factors for the various phases at 20 K are all close to 1, and, therefore, the spectral areas of the components can be regarded as satisfactory estimations for the iron content in the phases.

3.4. Chromium species and their sources

Amounts of total Cr and dissolved Cr(III) and Cr(VI) together with the concentration ratio of the dissolved Cr species to the total Cr are shown in Table 2. The relative uncertainty of the data for the chemical analysis was estimated to be below 10%. The total Cr concentrations were determined by proton-induced X-ray emission analysis for another section of the same filters (Salma et al., 2007). The masses given correspond to 9.1 m^3 of sampled air, and the total amounts represent mass concentrations of 0.04% and 0.05% for the $PM_{10-2.0}$ and $PM_{2.0}$ size fractions, respectively. The water soluble fraction of Cr in the joint (PM_{10}) size fractions was approximately 2.3% of the total Cr which is substantially smaller than the mean relative abundance and standard deviation of the water-soluble Cr in the PM_{10} size fraction of (12 ± 8)% for a kerbside site in Budapest. It is worth noting that the atmospheric concentration of Cr in the PM_{10} size fraction for the metro station was 5–6 times larger than for the city center (Salma and Maenhaut, 2006; Salma et al., 2007). These ambient values were obtained for an urban location that was very near to the subway station but for spring 2002. It was concluded from a comparative evaluation that the concentration level of Cr in central Budapest in springs was rising by 4–5% a year from 1996 to 2002 (Salma and Maenhaut, 2006), and, hence, its expected change between 2002 and 2006 is much smaller than the observed difference between the two environments. Joint comparison of Cr concentration and its water solubility within and outside the underground station, hence, implies that the water soluble amounts of Cr for the two environments were similar. This indicates that the increased negative health effects of aerosol particles in metros with respect to ambient outdoor particles should be related to further properties than their water solubility.

Nevertheless, the water solubility of Cr can be related to its source processes. It is also seen from Table 2 that the $PM_{2.0}$-fraction Cr was dissolved completely within the experimental uncertainty, while Cr in the $PM_{10-2.0}$ size fraction was partially soluble. The difference in the water solubility for the two size fractions indicates that the abundance of the major chemical forms of Cr is discrepant, and their source processes are diverse. The insoluble Cr, which was 2.7% of the total amount in the $PM_{10-2.0}$ size fraction, can partially be associated with some non-soluble Cr-compounds originating from the Earth's crust. Contribution of the crustal Cr was estimated similarly to Fe utilizing Eq. (1), and it was found to be at most 2–3% of the total Cr for the $PM_{10-2.0}$ size fraction. This means that Cr in the $PM_{10-2.0}$ size fraction was dominantly emitted into the air by mechanical disintegration of steel (Salma et al., 2007). The remaining insoluble Cr, i.e., at least approximately 24% of the total Cr in the $PM_{10-2.0}$ size fraction likely contains Cr_2O_3 and Cr in its elemental form. Chromium as an alloying element imparts to steels their resistance to corrosion by formation of a thin protective film of Cr_2O_3. These passive films are stable in normal atmospheric and aqueous environments, and withstand the corrosive action of sulphuric acid (Katz and Salem, 1994), and, therefore, the Cr_2O_3 on the steel particles could remain partially insoluble even during the digestion of the filters. Degradation of Cr-containing paints and Cr-plated surfaces could possibly contribute. At the same time, Cr in the $PM_{2.0}$-fraction particles was partially generated via vaporization by sparking between the electric conducting rail and collectors which could oxidize Cr(0) or Cr(III) emitted from the steel into their higher oxidation states including Cr(VI).

In the $PM_{10-2.0}$ size fraction, practically all dissolved Cr had an oxidation state of three, and the abundance of Cr(VI) was negligible with respect to Cr(III), and it was also close to the experimental uncertainty. This corresponds to ambient conditions where Cr(III) (which is an essential nutrient) occurs naturally since Cr(VI) is usually reduced to Cr(III) in fumes by combustion gases (Katz and Salem, 1994). In the $PM_{2.0}$ size fraction, however, approximately 93% of the dissolved Cr was present as Cr(III), and the rest, i.e., 7% consisted of Cr(VI). The last value can be of concern since Cr(VI) is one of the most harmful metallic components, and its occurrence is cautionary.

Table 2
Amount of total Cr, dissolved Cr(III) and Cr(VI) in ng for the aerosol filters, and the concentration ratio (Yield) of the dissolved Cr(III) and Cr(VI) to the total Cr for the $PM_{10-2.0}$ and $PM_{2.0}$ size fractions collected in a metropolitan underground railway station.

Size fraction	Total Cr[a]	Dissolved Cr(III)	Dissolved Cr(VI)	Yield
$PM_{10-2.0}$	434	315	0.5	0.73
$PM_{2.0}$	184	173	14	1.02

[a] Calculated from Salma et al. (2007).

4. Conclusions

The toxicity of metal-rich aerosol particles at high concentrations in workplace environments was documented and demonstrated in many studies (e.g., Ayres et al., 2008 and references therein). Water solubility of transition metals was identified as the main reason for their negative health effects. This is different for the underground railway systems since the metal-containing chemical species seem to be less water soluble. The adverse health effects are likely more related to surface chemistry influenced by the location and coordination of the metals on particle surfaces, perfection of the crystals on the particle surfaces, age of the aerosol particles and their surface size distribution than to the dissolved amounts. The present research demonstrates that the aerosol in an underground railway system differs not only in mass concentration levels, temporal variability and chemical composition especially in the $PM_{10-2.0}$ size fraction, and in mass size distribution from the ambient outdoor urban aerosol but substantial differences occur in chemical speciation and oxidation states of some relevant transition metals. Our knowledge on these properties is still insufficient. It has to be noted that the duration of the present pilot study was limited in time, and consequently, the results and conclusions derived cannot be generalized for longer times or seasons without additional research. It is highly desirable to conduct further comparative studies on the speciation of transition metals including Fe, Mn, Ni, Cu and Cr for urban and underground environments preferably with some toxicological research, and to compare the results because these collective interpretations can help us to understand the implications of aerosol particles for human health.

Acknowledgements

Financial support by the Hungarian Scientific Research Fund (contract K061193) is appreciated.

References

ATSDR (Agency for Toxic Substances and Disease Registry), 2000. Toxicological Profiles. US Public Health Service, Atlanta.

Ayres, J.G., Borm, P., Cassee, F.R., Castranova, V., Donaldson, K., Ghio, A., Harrison, R.M., Hider, R., Kelly, F., Kooter, I.M., Marano, F., Maynard, R.L., Mudway, I., Nel, A., Sioutas, C., Smith, S., Baeza-Squiban, A., Cho, A., Duggan, S.,

Froines, J., 2008. Evaluating the toxicity of airborne particulate matter and nanoparticles by measuring oxidative stress potential. Inhalation Toxicology 20, 75–99.
Chillrud, S.N., Epstein, D., Ross, J.M., Sax, S.N., Pederson, D., Spengler, J.D., Kinney, P., 2004. Elevated airborne exposures to manganese, chromium and iron of teenagers from steel dust and New York City's subway system. Environmental Science and Technology 38, 732–738.
Donaldson, K., Brown, D.M., Mitchell, C., Dinerva, M., Beswick, P.H., Gilmour, P., McNee, W., 1997. Free radical activity of PM_{10}: iron mediated generation of hydroxyl radicals. Environmental Health Perspectives 105, 1285–1289.
Gilmour, P.S., Brown, D.M., Lindsay, T.G., Beswick, P.H., MacNee, W., Donaldson, K., 1996. Adverse health effects of PM_{10} particles: involvement of iron in generation of hydroxyl radical. Occupational and Environmental Medicine 53, 817–822.
HEI (Health Effects Institute) Review Committee, 2002. Understanding the Health Effects of Components of the Particulate Matter: Progress and Next Steps. Health Effect Institute, Boston.
Karlsson, H.L., Nilsson, L., Möller, L., 2005. Subway particles are more genotoxic than street particles and include oxidative stress in cultured human lung cells. Chemical Research in Toxicology 18, 19–23.
Karlsson, H.L., Holgersson, Å., Möller, L., 2008. Mechanisms related to the genotoxicity of particles in the subway and from other sources. Chemical Research in Toxicology 21, 726–731.
Katz, S., Salem, H., 1994. The Biological and Environmental Chemistry of Chromium. Verlag Chemie, Wernheim.
Klencsár, Z., Kuzmann, E., Vértes, A., 1996. User-friendly software for Mössbauer-spectrum analysis. Journal of Radioanalytical and Nuclear Chemistry 210, 105–118.
Kopczewicz, B., Kopczewicz, M., 2002. Mössbauer study of iron containing atmospheric aerosol collected during the Chernobyl accident. Hyperfine Interactions 139/140, 657–665.
Kuzmann, E., Homonnay, Z., Nagy, S., Nomura, K., 2003. Mössbauer spectroscopy. In: Vértes, A., Nagy, S., Klencsár, Z. (Eds.), Handbook of Nuclear Chemistry, vol. 3. Kluver, Dordrecht, pp. 109–189.
Maenhaut, W., François, F., Cafmeyer, J., 1994. The "Gent" stacked filter unit sampler for the collection of atmospheric aerosols in two size fractions: description and instructions for installation and use. In: Applied Research on Air Pollution Using Nuclear-related Analytical Techniques. IAEA Report NAHRES-19. Vienna, pp. 249–263.
Mason, B., Moore, C.B., 1982. Principles of Geochemistry, fourth ed. Wiley, New York.
Nieuwenhuijsen, M.J., Gómez-Perales, J.E., Colvile, R.N., 2007. Levels of particulate air pollution, its elemental composition, determinants and health effects in metro systems. Atmospheric Environment 41, 7995–8006.
Pfeifer, G.D., Harrison, R.M., Lynam, D.R., 1999. Personal exposure to airborne metals in London taxi drivers and office workers in 1995 and 1996. Science of the Total Environment 235, 253–260.
Posta, J., Berndt, H., Lou, S.-K., Schaldach, G., 1993. High-performance flow flame atomic absorption spectrometry for automated on-line separation and determination of Cr(III)/Cr(VI) and preconcentration of Cr(VI). Analytical Chemistry 65, 2590–2595.
Salma, I., 2009. Air pollution in underground railway systems. In: Harrison, R.M., Hester, R. (Eds.), Issues in Environmental Science and Technology. Air Quality in Urban Environments, vol. 28. Royal Society of Chemistry Publishing, Cambridge, pp. 64–83.
Salma, I., Weidinger, T., Maenhaut, W., 2007. Time-resolved mass concentration, composition and sources of aerosol particles in a metropolitan underground railway station. Atmospheric Environment 41, 8391–8405.
Salma, I., Maenhaut, W., 2006. Changes in chemical composition and mass of atmospheric aerosol pollution between 1996 and 2002 in a Central European city. Environmental Pollution 143, 479–488.
Seaton, A., Cherrie, J., Dennekamp, M., Donaldson, K., Hurley, J.F., Tran, C.L., 2005. The London underground: dust and hazards to health. Occupational and Environmental Medicine 62, 355–362.
Sitzmann, B., Kendall, M., Watt, J., Williams, I., 1999. Characterisation of airborne particles in London by computer-controlled scanning electron microscopy. The Science of the Total Environment 241, 63–73.
Stevens, J.G., Stevens, V.E., 1969–1990. Mössbauer Effect Data Index. Hilger, London.
Vértes, A., Korecz, L., Burger, K., 1979. Mössbauer Spectroscopy. Elsevier, Amsterdam.
WHO (World Health Organization), 2000. Air Quality Guidelines for Europe. European series No. 91, second ed. WHO Regional Office for Europe, Copenhagen.